Designing High-Performance Multimode Fibers Using Refractive Index Optimization

Karthik Choutagunta, *Student Member, IEEE*, and Joseph M. Kahn, *Fellow, IEEE*

***Abstract*—The rich design landscape of optical fibers offers many opportunities for refractive index optimization. In particular, the refractive index profiles of multimode fibers (MMFs) and multicore fibers (MCFs) govern the behavior of spatial and polarization modes, including their bandwidth, mode count, mode coupling, modal dispersion, chromatic dispersion, and mode-dependent loss. In this article, we obtain update equations to optimize the shapes of fiber refractive index profiles for various applications using gradient descent. Starting with an initial fiber designed according to standard best practices, our methods iteratively modify the refractive index profile to improve upon the initial design. Interestingly, we see that optimization can sometimes yield large improvements in key fiber properties, such as a 20-fold reduction in the root-mean-square modal group delay spread, even though the index profile is changed very little from the initial design. We show that our methods can be used to tailor the mode coupling, modal dispersion and chromatic dispersion properties to desired values, and that optimization can be successfully applied over a large bandwidth. We provide illustrative design examples, including an optimization of a graded-index MMF with low group delay spread for long-haul mode-division-multiplexed transmission. Our algorithms can be used to design novel fibers or optimize existing fibers for next-generation transmission systems.**

***Index Terms*—Fiber design, modal dispersion, mode coupling, mode-division multiplexing, refractive index optimization.**

I. Introduction

OPTICAL fibers form the backbone of Internet infrastructure because they enable transmission of high-speed information signals over large distances. Since the advent of glass fibers, first proposed by Kao in 1966 [1] and demonstrated by Kapron, Keck, and Maurer in 1970 [2], the field of fiber design has rapidly evolved due to advances in low-loss fabrication and improvements in optical communication components [3]. The progress closely tracked the growing bandwidth requirements of optical transmission systems. Modern single-mode fibers have ultra-low losses of ∼0.154 dB/km and can support information capacities in excess of 881 Pb·km/s over the C+L wavelength band [4], [5]. The most advanced transmission systems today are based on mode-division multiplexing (MDM) in multimode fibers (MMFs) or multi-core fibers (MCFs), which increase capacity beyond that of single-mode fiber systems by using spatial and polarization modes to transmit data [6]–[8]. These systems use coherent detection with adaptive multiple-input multiple-output (MIMO) digitial signal processing at the receiver to compensate effects such as mode coupling, modal dispersion, and mode-dependent loss in the fiber and other link components [9]–[12]. This paper is mainly focused on optimal design of MMFs and MCFs with favorable modal characteristics, although the techniques we describe can also be applied to single-mode fiber design.

MMFs and MCFs have a rich design landscape because they have varied refractive index profile shapes, and can be made with different numerical apertures and core dimensions. The shape of the refractive index profile has a major impact on the properties of the guided modes. For example, the modes of step-index MMFs are weakly coupled, but they have a large group delay spread [13], [14]. The modes of parabolic (or graded-index) MMFs strongly couple with one another inside degenerate mode groups, and have reduced modal dispersion compared to step-index MMFs [15]. The addition of a lower-index trench or a depressed cladding has been shown to reduce the bending sensitivity of fibers and reduce mode-dependent loss [16]. Other types of MMFs include elliptical-core fibers [17], ring-core fibers [18], and rectangular-core fibers [19], just to name a few. In the case of MCFs, the design of each core and the spacing between the cores determines relevant parameters such as the amount of core-to-core coupling, group delay spread, effective areas and bend sensitivity [20]. MMFs and MCFs are typically designed to meet system design specifications that are unique to each application.

Numerical techniques such as shape and topology optimization have been widely applied to design mechanical components in the past [21]–[23], and have been used more recently in designing photonic components [24]–[28]. Inverse design methods allow "design by specification," whereby an algorithm uses local optimization methods based on convex optimization to efficiently search a large design space to find fabricable parameters that satisfy design criterion [29]. Adjoint methods allow large-scale photonics design by computing the gradient of an objective fuction with respect to all design degrees of freedom using two full-field electromagnetic simulations. These methods often result in nonintuitive topologies that attain superior functionality compared to their traditional counterparts. Computational optimization methods have been succesfully applied

Manuscript received January 23, 2020; revised June 17, 2020 and August 16, 2020; accepted September 3, 2020. Date of publication September 8, 2020; date of current version January 2, 2021. This work was supported by the Stanford Graduate Fellowship and Corning Inc. *(Corresponding author: Karthik Choutagunta.)*

The authors are with E. L. Ginzton Laboratory, Department of Electrical Engineering, Stanford University, Stanford, CA 94305 USA (e-mail: kchoutagunta@alumni.stanford.edu; jmk@ee.stanford.edu).

Color versions of one or more of the figures in this article are available online at https://ieeexplore.ieee.org.

Digital Object Identifier 10.1109/JLT.2020.3022636

TABLE I
OPPORTUNITIES FOR OPTIMIZATION-BASED FIBER DESIGN

Fiber Type	Loss	Chromatic Dispersion	Modal Dispersion	Mode Coupling	Bend Tolerance	Effective Area	Areal Density
LH single-mode fiber	Ultra-low	High *(want higher?)*	-	-	High	High *(want higher)*	Low
SR single-mode fiber	-	-	-	-	High	-	Medium *(want higher)*
LH CC-MCF	Ultra-low	High *(want higher?)*	Low *(want lower?)*	High	High	Very high *(want higher)*	Medium
SR UC-MCF	-	-	-	-	Low *(want higher?)*	-	Medium
LH MMF	Low *(want lower?)*	High *(want higher?)*	Moderate *(want lower?)*	Intragroup *(want intergroup)*	High	High	High
SR MMF for low-complexity MIMO	-	-	Moderate *(want lower?)*	Intragroup *(smaller mode groups?)*	High	-	High

to design various components such as wavelength splitters [29], Y-junctions [30], photonic switches [31], grating couplers [32], [33], multiplane light conversion-based mode multiplexers [34], and dispersion-compensating single-mode fibers [35]. Many commercial and open-source software packages already implement photonic waveguide design and optimization [36]–[39], but to the best of our knowledge, refractive index optimization tools that can control individual modal properties in MMFs and MCFs for MDM transmission systems are not readily available. Such tools would be of high interest to MDM practitioners because current state-of-the-art fibers are often designed by a brute-force grid search over a parameter space [40].

In this paper, we aim to contribute to this evolving field by proposing refractive index optimization methods to facilitate the efficient design of MMFs and MCFs. Our work is inspired by [35], where Riishede and Sigmund derived original gradient expressions for updating the refractive index profile of SMF to control the propagation constant and group velocity dispersion of the fundamental LP_{01} mode. We extend their approach to the multimode case, and show that similar expressions are effective in optimizing MMFs for various applications.

This paper is organized as follows. Section II presents the design landscape of a variety of optical fibers used for different purposes, and highlights opportunities for optimization-based design to create new fibers with better properties. Section III describes the optimization methods that can be used to control mode coupling, modal dispersion, and chromatic dispersion of fibers by modifying the fiber refractive index profile. Section IV presents some illustrative examples of fibers designed using our approach. Section V provides discussion and Section VI concludes the paper.

II. OPPORTUNITIES FOR OPTIMIZATION-BASED FIBER DESIGN

Table I summarizes the characteristics of typical optical fibers used for various applications. We categorize fibers as single-mode fibers, uncoupled-core and coupled-core multicore fibers (UC- and CC-MCFs), and multimode fibers (MMFs). These fibers can be used in either long-haul (LH) or short-reach (SR) transmission links. The optimal choice of transmission fiber depends on the specific demands of an application. The desired characteristics of loss, chromatic and modal dispersion, mode coupling, bend tolerance, modal effective areas, and areal density are all dependent on the type of fiber link. The opportunities for optimization-based design, i.e., the potential of numerical optimization of the refractive index to improve certain modal properties, are *italicized* in the table entries, and are also described below.

Single-mode fibers for LH transmission are usually composed of pure silica cores to enable transmission with ultra-low loss because signals need to propagate over thousands of kilometers [4]. The chromatic dispersion in these links is typically left uncompensated to mitigate nonlinear effects. Furthermore, the nonlinear coefficient scales inversely with the effective area of the fundamental LP_{01} mode. It may be desirable to increase both chromatic dispersion and modal effective area to improve nonlinear performance with the aid of refractive index optimization [41], [42]. In the case of short-reach single-mode fiber links for data center applications, where the nonlinearity of the fiber is less important than minimizing cross-sectional area, refractive index optimization may aid in the design of better fiber ribbons or bundles with improved bend tolerance and increased areal information density. While the design of optimized single-mode fibers is certainly of great practical importance, we believe that a brute-force grid search over the allowed design space is better than using the methods presented in this paper because the number of design variables in single-mode fiber design is relatively small.

MCFs, on the other hand, are more suitable for the refractive index optimization discussed in the next section because their refractive index profiles are parameterized by more design degrees of freedom, and optimization may help to find good values for these variables efficiently. CC-MCFs, whose cores are spaced close together to allow random strong mode coupling, are especially promising for LH MDM transmission because they have higher effective modal areas and superior nonlinear performance compared to parallel single-mode fibers. Modal dispersion in these fibers can be made low, which reduces the complexity of the required MIMO digital signal processing at the recevier. UC-MCFs do not have coupled cores, but they

allow transmission of many signals with low crosstalk in a more compact form factor compared to parallel single-mode fibers. Although optimized MCF design has been an active area of research and many research papers have studied the effects of the refractive index profile design using grid search [20], [43], [44], refractive index optimization methods may help to uncover novel designs that outperform state-of-the-art fibers.

MMFs are currently widely used in local-area and data-center networks due to the low cost and low energy consumption of MMF links. For example, vertical cavity surface emitting laser-based wavelength-division multiplexing links use OM4 and OM5 MMFs, which can be optimized for high effective modal bandwidths (EMBs) by tuning the alpha parameter of the graded-index refractive index profile [45], [46]. Since the EMB of MMFs can be increased by reducing the modal group delay spread, the optimization method presented in Section III-C can be used to improve the fiber design. The use of MMFs for MDM transmission is also an active research area because the capacity of MDM links increases proportionally to the number of propagating modes [47]. In the context of LH MDM links, MMFs should have low loss, low rms MD, strong intra- and inter-group mode coupling, and high modal effective areas [10], [48]. Short MMFs can be used for direct-detection MDM, where one of the goals in fiber design is to minimize mode coupling so that low-complexity optical MIMO equalization can be performed in the mode-group subspaces [49], [50]. Refractive index optimization is well suited for improving most of these MMF designs because their refractive index profiles are parameterized by a large number of design variables.

III. Design Algorithms

In this section, we provide optimization methods to control a small, but important, subset of fiber properties. Subsection III-A describes our high-level approach for using refractive index optimization in fiber design. Subsection III-B, III-C, III-D describe how to modify fiber refractive index profiles to control mode coupling, modal dispersion, chromatic dispersion, respectively.

A. Optimization Approach

Our overall approach for designing fibers using refractive index optimization is summarized in Fig. 1. We start with an initial two-dimensional refractive index profile $n_{\text{init}}(x, y)$ that guides D spatial and polarization modes. We solve a "forward" problem using a waveguide mode solver to obtain some key physical properties of the initial fiber. These properties may include its modal field patterns $\psi(x, y)$, propagation constants β, group delays τ, chromatic dispersion coefficients D, and modal effective areas A_{eff}. The optimization algorithm iteratively modifies the original refractive index profile using gradient descent to match a set of desired properties. The modifications during each iteration are typically small, although they can be chosen large if a large deviation from the initial design is desired. The update equations for some important parameters are obtained in the subsequent sections of this paper by extending the work from [35] to the multimode case. During each iteration, it is possible to enforce some design constraints, such as axial symmetry (for e.g., to produce round fibers) and maximum amplitude of the allowed index change. After a sufficient number of iterations, the fiber refractive index profile converges to $n_{\text{opt}}(x, y)$. These methods are not guaranteed to produce a globally optimal refractive index profile because $n_{\text{opt}}(x, y)$ depends on $n_{\text{init}}(x, y)$.

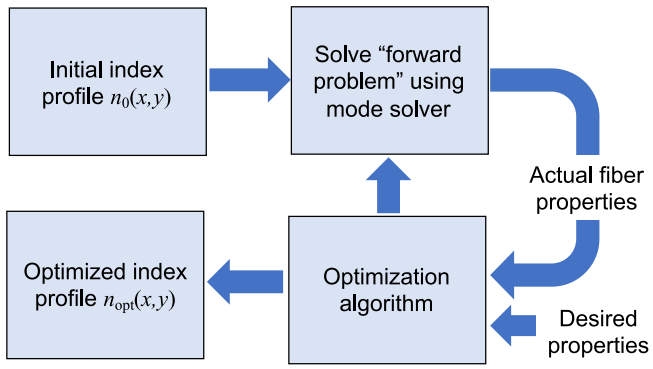

Fig. 1. Designing optical fibers using refractive index optimization. We start with an initial 2-dimensional refractive index profile $n_{\text{init}}(x, y)$ supporting D spatial and polarization modes and solve a forward problem using a mode solver to obtain the initial fiber's physical properties, which may include its mode fields $\psi^{(i)}(x, y)$, propagation constants, group delays, chromatic dispersion, and modal effective areas. The optimization algorithm iteratively modifies the original refractive index profile to match a set of desired properties. The optimized fiber refractive index profile is given by $n_{\text{opt}}(x, y)$.

B. Optimizing Modal Propagation Constant Degeneracies

Consider an initial refractive index profile $n_{\text{init}}(x, y)$ that supports D spatial and polarization modes at wavelength λ. The propagation constants of the modes are ordered as $\beta^{(1)} \leq \beta^{(2)} \leq \cdots \leq \beta^{(D)}$ (or equivalently in terms of effective modal indicies, $n_{\text{eff}}^{(1)} \leq \cdots \leq n_{\text{eff}}^{(D)}$, where $n_{\text{eff}}^{(i)} = \beta^{(i)}/k_0$ and $k_0 = 2\pi/\lambda$). Each propagation constant $\beta^{(i)}$ can be expanded using a Taylor series around a center angular frequency ω_0 as

$$\beta^{(i)} = \beta_0^{(i)} + \beta_1^{(i)}(\omega - \omega_0) + \frac{1}{2}\beta_2^{(i)}(\omega - \omega_0)^2 + \cdots, \quad (1)$$

where $\omega_0/\beta_0^{(i)}$ is the phase velocity, $1/\beta_1^{(i)}$ is the group velocity, and $\beta_2^{(i)}$ is the group velocity dispersion parameter of the i^{th} mode. Some of the modes may form mode groups, where modes within the same group have nearly degenerate β_0 and couple strongly with each other. Modes from different mode groups couple weakly with each other because their $\Delta\beta$ is large [51]. In this section, we aim to control the $\Delta\beta$ separation between modes to either create or remove propagation constant degeneracies. Additionally, we denote the transverse electric field profiles of all the modes by $\psi^{(1)}(x, y), \psi^{(2)}(x, y), \ldots, \psi^{(D)}(x, y)$. In this section, as well as in subsequent section III-C and III-D, we assume that the mode fields are normalized as $\iint \|\psi^{(i)}(x, y)\|^2 dxdy = 1$, similar to the normalization used in [35].

Without loss of generality, we desire to add refractive index updates to $n_{\text{init}}(x, y)$ such that the propagation constants are transformed to $\beta_{\text{des}}^{(1)} \leq \beta_{\text{des}}^{(2)} \leq \cdots \leq \beta_{\text{des}}^{(D)}$. When the refractive index profile is changed, it is possible that the transverse field profiles are also changed to $\psi_{\text{des}}^{(1)}, \psi_{\text{des}}^{(2)}, \ldots, \psi_{\text{des}}^{(D)}$. The desired

propagation constant spacing depends on the amount of mode coupling needed for a particular application, as discussed in Section II. We assign a cost function based on the squared differences between the actual and desired propagation constants:

$$J_{\text{coupling}} = \sum_{i=1}^{D} \left(\beta^{(i)} - \beta_{\text{des}}^{(i)}\right)^2. \tag{2}$$

A simple gradient descent method can iteratively update the refractive index profile at each spatial coordinate as

$$n(x,y) \leftarrow n(x,y) - \eta' \frac{\partial J_{\text{coupling}}}{\partial n(x,y)}, \tag{3}$$

where η' is a step-size parameter that should be chosen small enough such that perturbative modeling is valid. The gradient in (3) can be expanded in terms of the modal propagation constants as

$$\frac{\partial J_{\text{coupling}}}{\partial n(x,y)} = 2\sum_{i=1}^{D} \left(\beta^{(i)} - \beta_{\text{des}}^{(i)}\right) \cdot \frac{\partial \beta^{(i)}}{\partial n(x,y)}. \tag{4}$$

We rewrite and simplify the last factor in (4) using derivations from [35] as

$$\frac{\partial \beta^{(i)}}{\partial n(x,y)} = \frac{1}{2\beta^{(i)}} \frac{\partial \beta^{(i)2}}{\partial n(x,y)} = k_0^2 n(x,y) \frac{\left\|\psi^{(i)}(x,y)\right\|^2}{\beta^{(i)}}. \tag{5}$$

Combining (3)–(5), the refractive index update step can be succinctly expressed as

$$n(x,y) \leftarrow n(x,y) \times \left[1 - \eta \sum_{i=1}^{D} \left(\frac{\beta^{(i)} - \beta_{\text{des}}^{(i)}}{\beta^{(i)}}\right) \left\|\psi^{(i)}(x,y)\right\|^2\right], \tag{6}$$

where $\eta = 2\eta' k_0^2$ is an effective step size parameter that controls the amount of refractive index change per iteration in the optimization process.

Note that (6) is in a particularly interesting form: the refractive index update at a particular spatial coordinate is proportional to a weighted linear combination of the modal intensities at that location. The weights of this linear combination are the relative errors between the actual and desired propagation constants. Modes whose actual propagation constants are far away from their desired values contribute more to the refractive index update. To implement this optimization, we need to solve a "forward problem" using a waveguide mode solver to obtain the actual propagation constants and the modal transverse field profiles during each iteration.

C. Optimizing Modal Group Delay Spread

In this section, we describe a method to tailor the modal dispersion characteristics of an MMF or MCF. Specifically, we are given an initial D-mode fiber with refractive index profile $n_{\text{init}}(x,y)$ whose modes have uncoupled group delays $\tau^{(i)}(\lambda), i = 1, \ldots, D$, at a center wavelength λ. The group delays are usually specified in ps/m or ps/km units. They can be approximated as

$$\begin{aligned}\tau^{(i)}(\lambda) &= \left.\frac{\partial \beta^{(i)}}{\partial \omega}\right|_{\omega = 2\pi c/\lambda} \\ &\approx \frac{\beta^{(i)}(\lambda + \Delta\lambda) - \beta^{(i)}(\lambda - \Delta\lambda)}{2\Delta\omega} \\ &= \frac{\lambda^2}{\Delta\lambda}\left(\frac{\beta^{(i)}(\lambda + \Delta\lambda) - \beta^{(i)}(\lambda - \Delta\lambda)}{4\pi c}\right),\end{aligned} \tag{7}$$

where $\Delta\lambda$ is a small differential wavelength and c is the speed of light. Generally in fiber design, a goal is to minimize the root-mean-square (rms) uncoupled group delay spread. This is equivalent to minimizing the cost function

$$\begin{aligned}J_{\text{MD}} &= \left(\frac{1}{D}\sum_{i=1}^{D}\left[\tau^{(i)}(\lambda) - \bar{\tau}(\lambda)\right]^2\right)^{1/2}, \\ \bar{\tau}(\lambda) &= \frac{1}{D}\sum_{i=1}^{D}\tau^{(i)}(\lambda).\end{aligned} \tag{8}$$

We choose the rms metric rather than the peak-to-peak metric because the former is more useful when analyzing the performance of long-haul systems with strong mode coupling (see Section II-B of [52]).

The gradient of the group delays with respect to the refractive index profile is given by [35]

$$\frac{\partial \tau^{(i)}}{\partial n(x,y)} \propto n(x,y)\left(\frac{\left\|\psi^{(i)}(x,y,\lambda+\Delta\lambda)\right\|^2}{n_{\text{eff}}^{(i)}(\lambda+\Delta\lambda)} - \cdots \frac{\left\|\psi^{(i)}(x,y,\lambda-\Delta\lambda)\right\|^2}{n_{\text{eff}}^{(i)}(\lambda-\Delta\lambda)}\right), \tag{9}$$

where both $\beta^{(i)}$ and $\psi^{(i)}$ are written as functions of wavelength. Note that (9) is in an interesting form: the gradient of the group delays with respect to the refractive index at a spatial coordinate is minimized when the frequency variation of modal intensities at that location is also minimized. Intuitively, this makes sense because a fiber whose modal field patterns change very little as the frequency is varied will have less dispersion. It is straightforward to use (9) to compute the gradient of the uncoupled rms MD with respect to the refractive index profile:

$$\frac{\partial J_{\text{MD}}}{\partial n(x,y)} \propto \sum_{i=1}^{D}\left(\tau^{(i)} - \bar{\tau}\right)\left(\frac{\partial \tau^{(i)}}{\partial n(x,y)} - \frac{\partial \bar{\tau}}{\partial n(x,y)}\right). \tag{10}$$

Finally, we can reduce the uncoupled rms MD of the fiber by applying gradient descent:

$$n(x,y) \leftarrow n(x,y) - \eta'' \frac{\partial J_{\text{MD}}}{\partial n(x,y)}, \tag{11}$$

where η'' is the step size, which is usually chosen to be a small value. To implement this optimization, we are required to perform two forward passes of the waveguide mode solver at two closely spaced wavelengths per iteration.

D. Optimizing Chromatic Dispersion

It is also possible to use techniques similar to those in Section III-C to optimize chromatic dispersion in fibers. The dispersion coefficients $D^{(i)} \propto \beta_2^{(i)}$, typically measured in ps/nm · km units, are computed using the central difference approximation as [35],

$$D^{(i)} = -\frac{2\pi c}{\lambda^2}\frac{\partial^2 \beta^{(i)}}{\partial^2 \omega} \tag{12}$$

$$\approx \frac{-\lambda}{c}\frac{n_{\text{eff}}^{(i)}(\lambda+\Delta\lambda) - 2n_{\text{eff}}^{(i)}(\lambda) + n_{\text{eff}}^{(i)}(\lambda-\Delta\lambda)}{(\Delta\lambda)^2}, \tag{13}$$

and their gradients with respect to the index profile are [35]

$$\frac{\partial D^{(i)}}{\partial n(x,y)} \propto -n(x,y)\left(\frac{\left\|\psi^{(i)}(x,y,\lambda-\Delta\lambda)\right\|^2}{n_{\text{eff}}^{(i)}(\lambda-\Delta\lambda)} - \cdots 2\frac{\left\|\psi^{(i)}(x,y,\lambda)\right\|^2}{n_{\text{eff}}^{(i)}(\lambda)} + \frac{\left\|\psi^{(i)}(x,y,\lambda+\Delta\lambda)\right\|^2}{n_{\text{eff}}^{(i)}(\lambda+\Delta\lambda)}\right). \tag{14}$$

Similar to Section III-C, we observe that the above gradients are highest in spatial locations where the modal intensity patterns are changing fastest with frequency. The gradients in (14) could be used in a gradient descent method to increase or decrease mode-averaged or rms chromatic dispersion, depending on the desired effect in various applications.

IV. Design Examples

A. Strongly Coupled MMFs With Low Modal Dispersion

A major goal in designing MMFs for long-haul MDM transmission is to minimize the rms group delay of the propagating modes. It is a well-known fact that the end-to-end rms group delay in strongly coupled MDM links scales with the square root of the link length, and that the required receiver DSP complexity increases with the end-to-end rms group delay spread [9]. We show how the optimization algorithm presented in Section III-C can be used to reduce the rms group delay spread in MMFs.

As an example, we model the radial distribution of the refractive index $n_{\text{init}}(r)$ for an initial trench-assisted graded-index-core MMF that is designed to have low modal dispersion:

$$n_{\text{init}}(r) = \begin{cases} n_0\sqrt{1-2\Delta\,(r/a)^{\alpha}} & r < a \\ n_0\sqrt{1-2\Delta} - n_{\text{tr}} & a \le r < a + w_{\text{tr}} \\ n_0\sqrt{1-2\Delta}. & r \ge a + w_{\text{tr}} \end{cases} \tag{15}$$

We use similar fiber parameters as the rescaled 50-μ m profile from ref. [53]. The core radius is $a = 14\,\mu$m, the α parameter is 1.94, the core-cladding relative index difference is $\Delta = 0.0102$, and the trench has width $w_{\text{tr}} = 4\,\mu$m and depth $n_{\text{tr}} = 6 \times 10^{-3}$. We discretize $n_{\text{init}}(r)$ using 100 equidistant grid points and apply a finite-difference mode solver [54] to compute the modal properties at $\lambda = 1550$ nm. The initial fiber supports 15 spatial linearly polarized (LP) modes with an rms group delay of approximately 500 ps/km.[1] We then use a modal dispersion optimization algorithm to reduce the rms group delay of the initial MMF. We apply 200 iterations of the gradient descent step given by (9) in Section III-C. At each step of the optimization process, we update the radial refractive index distribution by at most 10^{-5}. The index updates are smoothed by a Gaussian low-pass filter[2] with a standard deviation width of 1 μm. The Gaussian low-pass filter also has the added benefit of preventing the optimization from becoming overly dependent on the exact mesh used when discretizing the refractive index profile, similar in purpose to the density filtering functions used by the authors in [35]. The resulting optimized MMF is described by $n_{\text{opt}}(r)$.

Fig. 2(a) and (b) show the difference between the initial and optimized radial refractive index distributions $n_{\text{opt}}(r) - n_{\text{init}}(r)$. The optimization does not change the original fiber very much because the maximum refractive index change is approximately 7×10^{-4}. The fiber is most changed in the core, and the deviation from the initial refractive index profile is similar to Fig. 1 from [55], where Petermann studied the optimal deviation from alpha law profiles to minimize dispersion in MMFs. Fig. 2(c) shows the modal effective indices of the optimized MMF offset from the cladding refractive index, $n_{\text{eff}} - n_{\text{clad}}$. It is evident that optimization does not introduce any new modes in the MMF. The 15 optimized modes are still well-confined since their effective indicies are above the cladding index n_{clad} by at least 2×10^{-3}, which should prevent excessive macrobend losses. The optimized modes are also still grouped into five distinct mode groups, and the modes within each mode group have $\Delta n_{\text{eff}} \ll 10^{-3}$, which should provide strong intramode coupling for long propagation distances. Fig. 2(d) shows the evolution of the modal group delays, expressed in ps/m units, during the optimization procedure. As seen in Fig. 2(e), the modes have an initial rms group delay of roughly 500 ps/km, which is reduced to ≈20 ps/km by the end of the optimization procedure.

We now study the precision required in controlling or measuring the refractive index profile of the preform during fiber fabrication using two different methods. In the first method, we use a simple sensitivity analysis to determine how tolerant the design is to scalar distortions. In Fig. 3(a), we compute the rms group delay achieved by a fiber with refractive index profile given by

$$n_{\text{init}}(r) + f \cdot \left(n_{\text{opt}}(r) - n_{\text{init}}(r)\right), \tag{16}$$

where f is a rescaling parameter that controls the deviation from the optimal index change $n_{\text{opt}}(r) - n_{\text{init}}(r)$. The special

[1] We have tried our best to replicate low-MD fibers from past literature, but our initial refractive index values may be slightly different from those reported in ref. [53] Small variations in the modelled refractive index distribution, discretization of the grid, and choice of mode solver can lead to different initial rms group delays. Our goal here is to show the efficacy of refractive index optimization starting from a relatively good initial fiber design.

[2] We note that our current implementation of MMF refractive index optimization applies low-pass filtering to the index updates as a post-processing step. Although this is a suboptimal approach, we have not observed any oscillations and our designs always appear to converge to the same local minima. A better technique is to incorporate the smoothing filter directly into the gradient calculations via the chain rule. We may consider doing this in future work.

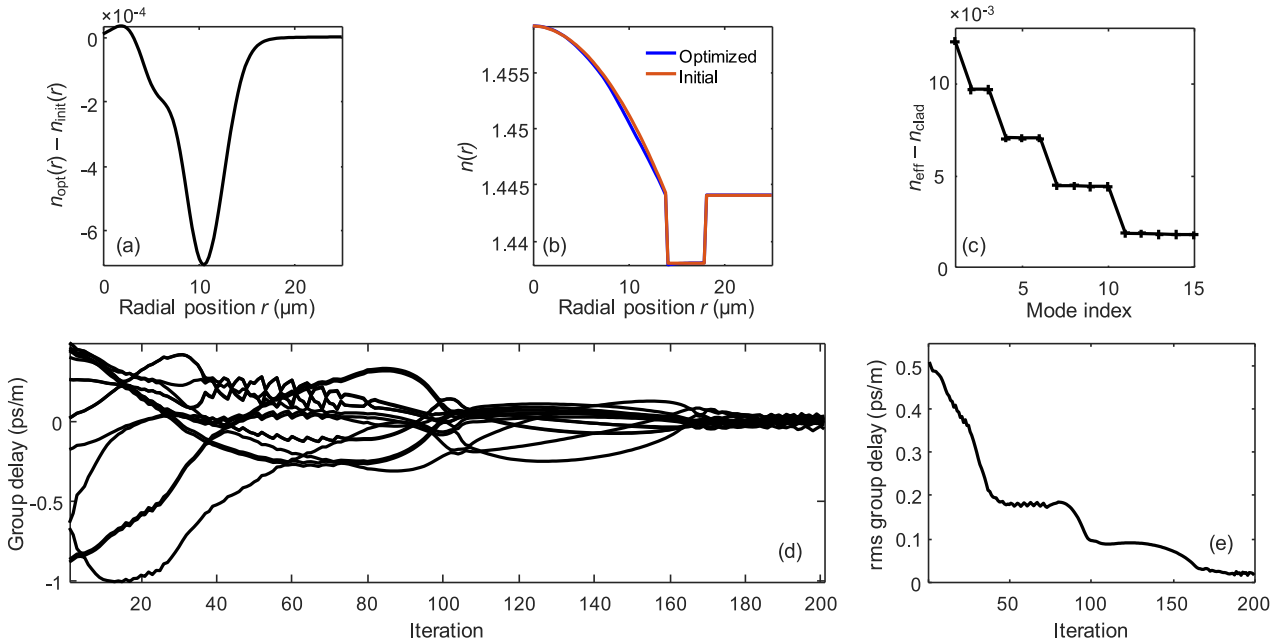

Fig. 2. Reducing the group delay spread in a graded-index MMF, which is similar to the rescaled 50-μ m fiber from ref. [53]. The MMF supports 15 LP modes at 1550 nm, has a core radius of $a = 14\,\mu$m, an α value of 1.94, a trench of width 4 μm and depth $\Delta n = 6 \times 10^{-3}$. The refractive index optimization procedure was run for 200 iterations, and at each iteration the radial distribution of the refractive index profile was changed by at most 10^{-5}. The resulting change between the initial and optimized refractive index distributions is shown in (a), and the initial and optimizized refractive index profiles are shown in (b). The effective indicies (offset from the cladding index) of all 15 modes of the optimized MMF are shown in (c). An overlay of the evolutions of all the group delays in the MMF throughout the optimization process is shown in (d), and the corresponding rms group delay evolution is shown in (e).

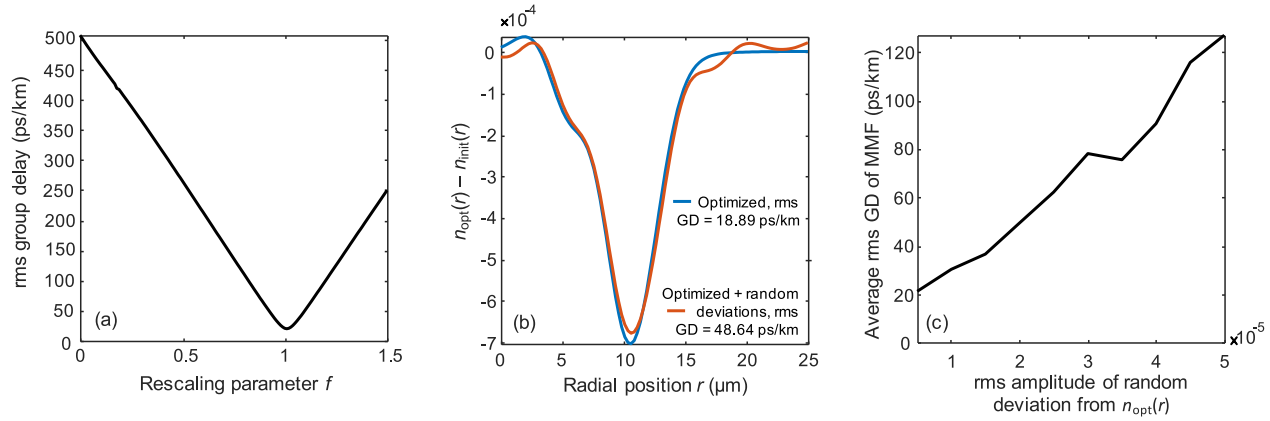

Fig. 3. (a) Sensitivity of the achieved rms group delay to a deviation from the optimized refractive index change. There is no deviation from the optimized refrative index profile when the rescaling parameter is chosen as $f = 1$. (b) Example of an optimized MMF refractive index profile with and without a random deviation resulting from imperfect fabrication. (c) The average rms GD of MMFs increases with the rms amplitude of random errors to the optimized refractive index profile.

case of $f = 0$ degenerates to the initial design (rms group delay 500 ps/km) whereas $f = 1$ corresponds to the optimized index profile (rms group delay 20 ps/km). It can be seen that if the refractive index is controlled to within $0.82 \leq f \leq 1.2$, then the achievable rms group delay can be kept under 100 ps/km. This requirement is equivalent to being able to measure the refractive index profile to within

$$\begin{aligned}\Delta n &\leq (1.2 - 0.82) \times \max\left(n_{\text{opt}}(r) - n_{\text{init}}(r)\right) \\ &= 2.7 \times 10^{-4}. \end{aligned} \tag{17}$$

In the second method, we study how tolerant the fiber design is to additive random deviations from the optimal radial index profile. We generate these deviations as smooth zero-mean curves using

$$\delta n(r) = \sum_{i=1}^{N} A_i \cos(2\pi f_i r + \phi_i) + B_i \sin(2\pi f_i r + \theta_i), \tag{18}$$

where N is the number of sinusoids used in the expansion of the random deviation, f_i are the spatial frequencies, A_i and B_i are the amplitudes of each spatial frequency, and ϕ_i and θ_i are random phase offsets. In our simulations, we produce random

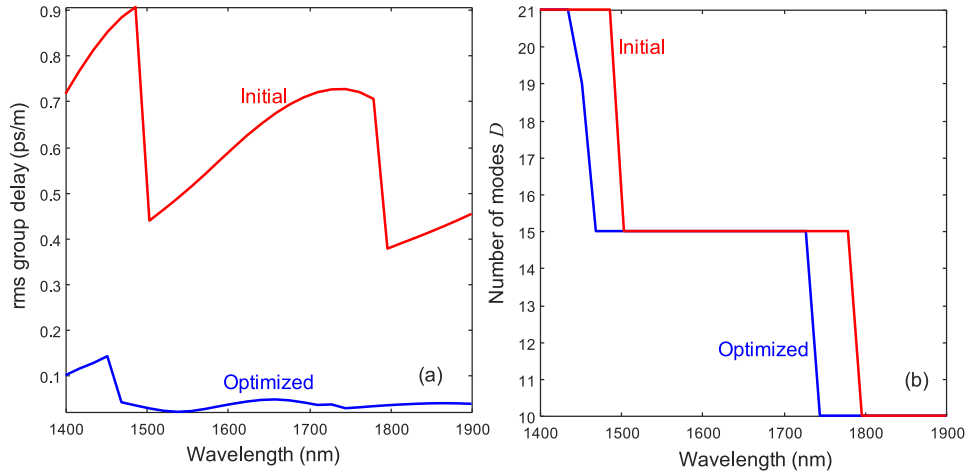

Fig. 4. (a) The rms group delay of the initial and optimized MMFs as the wavelength is varied from 1400 nm to 1900 nm. (b) The number of modes D supported by the initial and optimized MMFs in the same wavelength range.

deviations by using $N = 5$ terms, f_i linearly spaced from $0\,\mathrm{m}^{-1}$ to $25 \times 10^4\,\mathrm{m}^{-1}$, and ϕ_i and θ_i are uniformly distributed from 0 to 2π radians. A_i and B_i are chosen from a zero-mean Gaussian distribution with unit variance and then scaled such that $\delta n(r)$ is of a desired rms amplitude. Fig. 3(b) shows an example of this type of additive random deviation to the optimized index profile. The blue curve, reproduced from Fig. 2(a), corresponds to the optimal profile and the optimal MMF has an rms group delay of roughly 20 ps/km. The amber curve corresponds to a MMF with a random deviation $\delta n(r)$ of rms amplitude 2×10^{-5}, and this MMF has an rms group delay of roughly 50 ps/km. In Fig. 3(c), we sweep over a range of rms amplitudes for the random deviation added to $n_{\mathrm{opt}}(r)$ to study the extent of increase in rms group delay. At each rms amplitude, we simulate 20 MMFs with independently generated $\delta n(r)$ and compute the average rms group delay of the realized MMFs. We observe that to keep the rms group delay of the MMF below 100 ps/km (recall the original unoptimzed MMF has an rms group delay of 500 ps/km), it is necessary to control the errors in the fiber preform's refractive index profile to less than 4.2×10^{-5}. This is a stricter limit than that suggested by (17) because random additive deviations can change the optimal profile in more ways than a rescaling operation.

Although a fabricated fiber can differ from the optimized design in many ways and we have only considered two simplified methods of computing the necessary precision in controlling the fiber preform in this paper, we nevertheless see that numerical optimization is robust to manufacturing errors.

Fig. 4(a) shows the variation of the rms group delay of the initial and optimized MMFs with wavelengths in the range from 1400 nm to 1900 nm. There is a discontinuity in the rms group delay curve corresponding to the initial MMF at cutoff wavelengths ~ 1503 nm and ~ 1780 nm because, as seen from Fig. 4(b), the fiber supports more modes ($D = 21$) below 1503 nm and fewer modes ($D = 10$) above 1780 nm. The corresponding cutoff wavelengths for the optimized fiber are slightly shifted, and occur at ~ 1469 nm and ~ 1728 nm. Regardless, while the initial MMF has rms group delay > 488 ps/km for all wavelengths in the C-band (1530 – 1565 nm), the optimized MMF has group delays < 25 ps/km. This represents an almost $20-$fold improvement in the rms group delay spread due to refractive index optimization. Optimized MMFs with such low group delay spreads are suitable for ultra-long-haul MDM links using coherent detection because the adaptive DSP in the receiver can use fewer equalization taps.

B. *Transformation of a Ring-Core MMF to a CC-MCF*

In this section, we use the mode coupling control algorithm from Section III-B to modify the propagation constants of a ring-core fiber (RCF). We show that an RCF converges to a coupled-core multicore fiber (CC-MCF) when the effective indices of the modes are pushed closer together (i.e., when they are made degenerate). Here, our intention is not to create a novel fiber, but rather to demonstrate refractive index optimization behavior using an intuitive example.

We start with an initial RCF, similar to fibers studied in ref. [18]. Using the same notation as [18], we choose the outer ring radius $a = 7\,\mu$m (measured from the center of the fiber), and inner ring radius $d/2 = 2.1\,\mu$m, such that $d/2a = 0.3$. The relative index difference between the ring and the cladding is chosen to be $\Delta = 0.8\%$. The ring is assumed to have a constant refractive index, and so there is a sharp transition at the boundary between the ring and cladding. We discretize the initial refractive index distribution $n_{\mathrm{init}}(x, y)$ using a 100×100 grid with $0.2\,\mu$m spacing in both in the x and y directions. The initial RCF index profile $n_{\mathrm{init}}(x, y)$ is shown in Fig. 5(b). At 1550 nm, this RCF supports 5 spatial modes, whose intensity profiles are shown in Fig. 5(e). The effective indicies of these modes are $n_{\mathrm{eff}} - n_{\mathrm{clad}} \approx 4 \times 10^{-3}$ (two modes), 7×10^{-3} (two modes), and 8.5×10^{-3} (one mode). These modes are well-confined inside the ring (since their $n_{\mathrm{eff}} \gg n_{\mathrm{clad}}$), and moreover they form three mode groups with weak intergroup coupling (since $\Delta n_{\mathrm{eff}} \geq 1.5 \times 10^{-3}$ between modes in different mode groups).

Now, we apply an optimization method to make the fiber modes degenerate. We perform 380 iterations of the gradient

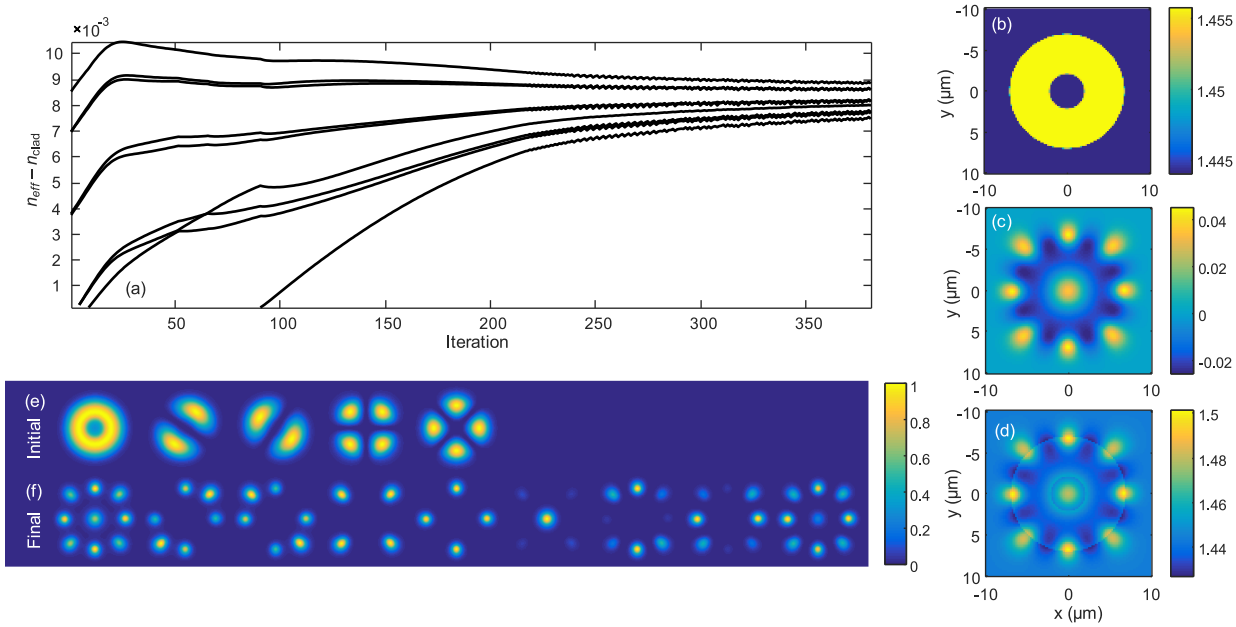

Fig. 5. An initial RCF with 5 spatial modes, modelled using parameters from [18] is transformed into a CC-MCF when the modal propagation constants are pushed closer together (i.e. made nearly degenerate). The initial step index RCF has core radius $a = 7$ μm, a relative index difference of $\Delta = 0.8\%$, and a ring inner-diameter-to-outer-diameter ratio of $d/2a = 0.3$. The refractive index optimization was run for 380 iterations, and the refractive index profile was changed at each spatial coordinate by at most $\Delta n = 2 \times 10^{-4}$ during each step. The evolution of the modal effective indicies (offset from the cladding index) is shown in (a). The initial refractive index of the RCF $n_{\text{init}}(x, y)$ is shown in (b), the refractive index change produced by the optimization is shown in (c), and the resulting refractive index distribution $n_{\text{opt}}(x, y)$, which resembles that of a nine-core CC-MCF, is shown in (d). The modal field intensity patterns of the initial RCF and the resulting CC-MCF are shown in (e) and (f), respectively.

descent step given by (6). During each iteration, the propagation constant corresponding to the lowest-order mode is kept constant (equal to $\beta_{\text{des}}^{(1)} \approx k_0 n_{\text{core}}$) and the spread of the desired modal propagation constants $\beta_{\text{des}}^{(i)}$ is reduced by a factor of 2. This causes the current propagation constants $\beta^{(i)}$ to move closer to the $\beta_{\text{des}}^{(i)}$ and eventually converge to $k_0 n_{\text{core}}$. Each iteration changes the refractive index profile by a maximum step size of 2×10^{-4}. This is larger than the step size used in Section IV-A for group delay reduction because larger index changes are required to change modal propagation constants. We do not enforce axial symmetry constraints, and so each spatial coordinate (i.e., each (x, y) grid point) is allowed to evolve independently.

Fig. 5(a) shows the evolution of the modal effective indicies (offset from the cladding index) during the optimization process. Initially there is a large spread in the propagation constants, but the spread becomes smaller as the optimization progresses. Although the initial RCF has five spatial modes, four new modes are added at iterations 5, 9 and 81 because the fiber is being changed drastically. Fig. 5(c) shows the total index difference $n_{\text{opt}}(x, y) - n_{\text{init}}(x, y)$, and Fig. 5(d) shows the final optimized profile $n_{\text{opt}}(x, y)$. It is interesting to see that the optimization method tries to convert the RCF into a CC-MCF with nine cores. Whereas the design example from Section IV-A is a small perturbation to the initial design, this example shows a drastic transformation from one fiber type to another. The low-index region inside the initial ring has been replaced by a central high-index core, and the annular region has been converted into eight equally spaced cores. The intensity profiles of the modes supported by the final CC-MCF are shown in Fig. 5(f). Since these modes are mostly confined to the high-index cores, it makes sense that they would all have roughly the same propagation constants, as seen in Fig. 5(a).

The path taken by refractive index optimization is highly dependent on the initial fiber design, the gradient update step size, and the distribution of the modal patterns. However, we can try to understand why the RCF converges to a CC-MCF by looking at the form of Eq. (6). As discussed in Section III-B, the refractive index updates are concentrated in spatial locations where the modal intensities are the highest. The high-order modal intensity patterns of the initial RCF, shown in Fig. 5(e), have lobes with distinct peaks spaced along the annular region, and so the updates form cores in those locations. As the optimization progresses, and the supported modes become more confined within these cores, the gradient updates increase the index contrast between the cores and the surrounding cladding, which confines the modes even more. This positive feedback loop promotes the synthesis of a CC-MCF structure.

V. Discussion

Although we have only discussed two fiber design examples in Section IV, Table I shows that refractive index optimization has a large scope and that it can potentially be applied to a wider variety of fibers. Here, we discuss some limitations of our approach and also comment on various ideas and extensions that can be implemented in future research.

The success of our proposed methods largely depends on the initial refractive index profile $n_{\text{init}}(x, y)$. This is because our methods apply gradient descent to minimize a cost function

even though refractive index optimization is inherently non-convex in nature. Therefore, $n_{\mathrm{opt}}(x, y)$ might converge to index profiles corresponding to local minima. In practice, one might have to test multiple values of $n_{\mathrm{init}}(x, y)$ and pick $n_{\mathrm{opt}}(x, y)$ with the lowest cost (i.e., with the best modal characteristics). Optimization hyperparameters, such as the index update step size and number of iterations, are currently chosen heuristically, but further research is required to understand how they influence the evolution of the index profile. Smaller step sizes with more iterations allow the index profile to adiabatically transition into $n_{\mathrm{opt}}(x, y)$, resulting in possibly lower cost, whereas larger step sizes with fewer iterations allow the fiber to escape local minima. Advanced schemes based on variable-rate step-size decay can possibly outperform standard gradient descent, but we have not evaluated such methods in this paper.

The number of modes guided by the fiber can change during the refractive index optimization process because the refractive index is being continuously changed. For example, while the low group-delay MMF from Section IV-A had 15 spatial modes throughout the optimization because $n_{\mathrm{opt}} - n_{\mathrm{init}}$ is small, the number of guided modes in the RCF from Section IV-B was not constant because the refractive index change is relatively large. Furthermore, it can be observed from Fig. 3(c) that the wavelengths where new modes are guided and modes are cutoff are different for the initial and optimized fibers. These effects can be problematic in applications where it is desired to keep the number of guided fiber modes constant across a wavelength band. Although we have not fully investigated methods to conserve the number of modes in this paper, possible approaches include: (i) imposing constraints on the total allowed index change $n_{\mathrm{opt}} - n_{\mathrm{init}}$, (ii) rescaling the core and cladding dimensions after each iteration, and (iii) increasing or decreasing the number of modes guided by n_{init} so that n_{opt} has the desired number of modes.

In this paper, we make the simplifying assumption that material dispersion arises only from a pure silica cladding. We capture material dispersion effects by using the Sellmeier equation with fitting parameters for fused silica inside both the core and cladding [56]. The refractive index profile of the core is added as an offset and is assumed to have the same wavelength dependence as the cladding. However, in practice, fused silica cores are doped with germanium to raise the core index above the cladding index, and with fluorine to decrease it below the cladding index. Although we believe the impact of our simplying assumption is small, the wavelength dependence of our model can nevertheless be improved by appropriate reweighting of the Sellmeier equation coefficients with parameters for germanium and fluorine.

Other important research directions include deriving gradient-based methods for controlling key optical fiber properties besides mode coupling and dispersion. For example, properties such as bend tolerance and effective modal areas, which depend on how tightly the modes are confined inside the core, can be optimized by tuning the numerical aperture and the trench volume at the core/cladding boundary. Joint optimization of multiple objectives can also be investigated by adding multiple weighted terms to a cost function. Fabrication and experimental testing of optimized fibers are important next steps.

VI. Conclusion

In this paper, we studied the problem of using optimization of refractive index profiles to design better MMFs and MCFs. We proposed an iterative optimization method based on gradient descent to steer fiber properties toward their desired values. We obtained analytical update equations to control key fiber properties, including modal propagation constants, modal group delays, and mode-dependent chromatic dispersion. Using a numerical simulation, we demonstrated that a small changes to the index profile of a 15-spatial mode trench-assisted graded-index-core MMF can reduce its rms group delay spread by $20-$fold across a wide range of wavelengths. Further applications of this research include fabrication and experimental measurement of optimized fibers, as well as designing novel fibers for MDM transmission.

Acknowledgment

Discussions with Ming-Jun Li are acknowledged.

References

[1] K. C. Kao and G. A. Hockham, "Dielectric-fibre surface waveguides for optical frequencies," *Proc. IEEE*, vol. 113, no. 7, pp. 1151–1158, Jul. 1966.
[2] F. P. Kapron, D. B. Keck, and R. D. Maurer, "Radiation losses in glass optical waveguides," *Appl. Phys. Lett.*, vol. 17, no. 10, pp. 423–425, 1970.
[3] M. Li and D. A. Nolan, "Optical transmission fiber design evolution," *J. Lightw. Technol.*, vol. 26, no. 9, pp. 1079–1092, May 2008.
[4] J. D. Downie, M.-J. Li, and S. Makovejs, *Single-Mode Fibers for High Speed and Long-Haul Transmission*. Singapore: Springer Singapore, 2018, pp. 1–37.
[5] J.-X. Cai *et al.*, "51.5 Tb/s capacity over 17,107 km in C+L bandwidth using single-mode fibers and nonlinearity compensation," *J. Lightw. Technol.*, vol. 36, no. 11, pp. 2135–2141, Jun. 2018.
[6] R. Ryf *et al.*, "Mode-division multiplexing over 96 km of few-mode fiber using coherent 6×6 MIMO processing," *J. Lightw. Technol.*, vol. 30, no. 4, pp. 521–531, Feb. 2012.
[7] P. J. Winzer, "Making spatial multiplexing a reality," *Nature Photon.*, vol. 8, no. 5, pp. 345–348, 2014.
[8] D. A. A. Mello, H. Srinivas, K. Choutagunta, and J. M. Kahn, "Impact of polarization- and mode-dependent gain on the capacity of ultra-long-haul systems," *J. Lightw. Technol.*, vol. 38, no. 2, pp. 303–318, Jan. 2020.
[9] S. Ö. Arik, D. Askarov, and J. M. Kahn, "Adaptive frequency-domain equalization in mode-division multiplexing systems," *J. Lightw. Technol.*, vol. 32, no. 10, pp. 1841–1852, May 2014.
[10] K. Choutagunta and J. M. Kahn, "Dynamic channel modeling for mode-division multiplexing," *J. Lightw. Technol.*, vol. 35, no. 12, pp. 2451–2463, Jun. 2017.
[11] K. Choutagunta, I. Roberts, and J. M. Kahn, "Efficient quantification and simulation of modal dynamics in multimode fiber links," *J. Lightw. Technol.*, vol. 37, no. 8, pp. 1813–1825, Apr. 2019.
[12] K. Choutagunta *et al.*, "Modal dynamics in spatially multiplexed links," in *Proc. Opt. Fiber Commun. Conf.*, Mar. 2019, pp. 1–3.
[13] J. Carpenter, B. C. Thomsen, and T. D. Wilkinson, "Degenerate mode-group division multiplexing," *J. Lightw. Technol.*, vol. 30, no. 24, pp. 3946–3952, Dec. 2012.
[14] A. Snyder and J. Love, *Optical Waveguide Theory*. Berlin, Germany: Springer, 2012.
[15] D. Gloge and E. A. J. Marcatili, "Multimode theory of graded-core fibers," *Bell Syst. Tech. J.*, vol. 52, no. 9, pp. 1563–1578, Nov. 1973.
[16] D. Molin, M. Bigot-Astruc, K. de Jongh, and P. Sillard, "Trench-assisted bend-resistant om4 multi-mode fibers," in *Proc. Eur. Conf. Opt. Commun.*, Sep. 2010, pp. 1–3.
[17] G. Milione *et al.*, "MIMO-less space division multiplexing with elliptical core optical fibers," in *Proc. Opt. Fiber Commun. Conf.*, Mar. 2017, pp. 1–3.
[18] M. Kasahara *et al.*, "Design of three-spatial-mode ring-core fiber," *J. Lightw. Technol.*, vol. 32, no. 7, pp. 1337–1343, Apr. 2014.

[19] L. Rechtman and D. M. Marom, "Rectangular versus circular fiber core designs: New opportunities for mode division multiplexing?" in *Proc. Opt. Fiber Commun. Conf.*, Mar. 2017, pp. 1–3.
[20] S. Ö. Arik and J. M. Kahn, "Coupled-core multi-core fibers for spatial multiplexing," *IEEE Photon. Technol. Lett.*, vol. 25, no. 21, pp. 2054–2057, Nov. 2013.
[21] M. P. Bendsoe and N. Kikuchi, "Generating optimal topologies in structural design using a homogenization method," *Comput. Methods Appl. Mech. Eng.*, vol. 71, no. 2, pp. 197–224, 1988.
[22] M. P. Bendsoe and O. Sigmund, *Topology Optimization: Theory, Methods, and Applications*, 2nd ed. Berlin, Germany: Springer-Verlag, 2004.
[23] T. Borrvall and J. Petersson, "Topology optimization of fluids in stokes flow," *Int. J. Numer. Methods Fluids*, vol. 41, no. 1, pp. 77–107, 2003.
[24] J. S. Jensen and O. Sigmund, "Topology optimization for nano-photonics," *Laser. Photon. Rev.*, vol. 5, no. 2, pp. 308–321, 2011.
[25] P. Seliger, M. Mahvash, C. Wang, and A. F. J. Levi, "Optimization of aperiodic dielectric structures," *J. Appl. Phys.*, vol. 100, no. 3, 2006, Art. no. 034310.
[26] W. R. Frei, D. A. Tortorelli, and H. T. Johnson, "Geometry projection method for optimizing photonic nanostructures," *Opt. Lett.*, vol. 32, no. 1, pp. 77–79, Jan. 2007.
[27] V. Liu and S. Fan, "Compact bends for multi-mode photonic crystal waveguides with high transmission and suppressed modal crosstalk," *Opt. Express*, vol. 21, no. 7, pp. 8069–8075, Apr. 2013.
[28] G. Veronis, R. W. Dutton, and S. Fan, "Method for sensitivity analysis of photonic crystal devices," *Opt. Lett.*, vol. 29, no. 19, pp. 2288–2290, Oct. 2004.
[29] A. Y. Piggott, J. Lu, K. G. Lagoudakis, J. Petykiewicz, T. M. Babinec, and J. Vukovi, "Inverse design and demonstration of a compact and broadband on-chip wavelength demultiplexer," *Nature Photon.*, vol. 9, no. 6, pp. 374–377, May 2015.
[30] C. M. Lalau-Keraly, S. Bhargava, O. D. Miller, and E. Yablonovitch, "Adjoint shape optimization applied to electromagnetic design," *Opt. Express*, vol. 21, no. 18, pp. 21 693–21 701, Sep. 2013.
[31] Y. Elesin, B. Lazarov, J. Jensen, and O. Sigmund, "Design of robust and efficient photonic switches using topology optimization," *Photon. Nanostructures - Fundam. Appl.*, vol. 10, no. 1, pp. 153–165, 2012.
[32] A. C. R. Niederberger, D. A. Fattal, N. R. Gauger, S. Fan, and R. G. Beausoleil, "Sensitivity analysis and optimization of sub-wavelength optical gratings using adjoints," *Opt. Express*, vol. 22, no. 11, pp. 12 971–12 981, Jun. 2014.
[33] L. Su, R. Trivedi, N. V. Sapra, A. Y. Piggott, D. Vercruysse, and J. Vučković, "Fully-automated optimization of grating couplers," *Opt. Express*, vol. 26, no. 4, pp. 4023–4034, Feb. 2018.
[34] N. K. Fontaine, R. Ryf, H. Chen, D. T. Neilson, K. Kim, and J. Carpenter, "Laguerre-gaussian mode sorter," *Nature Commun.*, vol. 10, no. 1, pp. 1–7, Apr. 2019.
[35] J. Riishede and O. Sigmund, "Inverse design of dispersion compensating optical fiber using topology optimization," *J. Opt. Soc. Amer. B*, vol. 25, no. 1, pp. 88–97, Jan. 2008.
[36] L. Su, D. Vercruysse, J. Skarda, N. V. Sapra, J. A. Petykiewicz, and J. Vuckovic, "Nanophotonic inverse design with SPINS: Software architecture and practical considerations," *Applied Phys. Rev.*, vol. 7, no. 1, American Institute of Physics, Mar. 2020.
[37] *Lumerical MODE*, 2020. [Online]. Available: https://www.lumerical.com/products/mode
[38] *COMSOL wave optics software for analyzing micro- and nano-optical devices*, 2020. [Online]. Available: https://www.comsol.com/wave-optics-module
[39] *VPIcomponentMaker fiber optics*, 2020. [Online]. Available: https://www.vpiphotonics.com/Tools/FiberOptics/
[40] X. Chen, M. J. Li, and D. R. Powers, "Multimode optical fiber and systems comprising such fiber," U.S. Patent 8 971 683B2, Mar. 3, 2015.
[41] A. Carena *et al.*, "Novel figure of merit to compare fibers in coherent detection systems with uncompensated links," *Opt. Express*, vol. 20, no. 1, pp. 339–346, Jan. 2012.
[42] M. Bigot-Astruc and P. Sillard, "Realizing large effective area fibers," in *Proc. Opt. Fiber Commun. Conf.*, Mar. 2012, pp. 1–3.
[43] B. Huang *et al.*, "Minimizing the modal delay spread in coupled-core two-core fiber," in *Proc. CLEO*, Jun. 2016, pp. 1–2.
[44] K. Saitoh and S. Matsuo, "Multicore fiber technology," *J. Lightw. Technol.*, vol. 34, no. 1, pp. 55–66, Jan. 2016.
[45] D. Molin, M. Bigot-Astruc, A. Amezcua-Correa, and P. Sillard, "Recent advances on MMFs for WDM and MDM," in *Proc. Opt. Fiber Commun. Conf.*, Mar. 2018, pp. 1–3.
[46] D. Molin, F. Achten, M. Bigot, A. Amezcua-Correa, and P. Sillard, "Wideband OM4 multi-mode fiber for next-generation 400 Gbps data communications," in *Proc. Eur. Conf. Opt. Commun.*, Sep. 2014, pp. 1–3.
[47] R. Ryf *et al.*, "High-spectral-efficiency mode-multiplexed transmission over graded-index multimode fiber," in *Proc. Eur. Conf. Opt. Commun. Post Deadline Session*, Sep. 2018, pp. 1–3.
[48] D. W. Peckham, Y. Sun, A. McCurdy, and R. Lingle, "Chapter 8 - few-mode fiber technology for spatial multiplexing," in *Optical Fiber Telecommunications (Sixth Edition)*, (Optics and Photonics Series), I. P. Kaminow, T. Li, and A. E. Willner, Eds. New York, NY, USA: Academic Press, 2013, pp. 283–319.
[49] K. Choutagunta, I. Roberts, D. A. B. Miller, and J. M. Kahn, "Adapting Mach-Zehnder mesh equalizers in direct-detection mode-division-multiplexed links," *J. Lightw. Technol.*, vol. 38, no. 4, pp. 723–735, Feb. 2020.
[50] S. Ö. Arik and J. M. Kahn, "Direct-detection mode-division multiplexing in modal basis using phase retrieval," *Opt. Lett.*, vol. 41, no. 18, pp. 4265–4268, 2016.
[51] D. Marcuse, *Theory of Dielectric Optical Waveguides*, 1st ed. New York, NY, USA: Academic, 1974.
[52] K. Choutagunta, S. Ö. Arik, K.-P. Ho, and J. M. Kahn, "Characterizing mode-dependent loss and gain in multimode components," *J. Lightw. Technol.*, vol. 36, no. 18, pp. 3815–3823, Sep. 2018.
[53] P. Sillard *et al.*, "Low-differential-mode-group-delay 9-LP-mode fiber," *J. Lightw. Technol.*, vol. 34, no. 2, pp. 425–430, Jan. 2016.
[54] A. B. Fallahkhair, K. S. Li, and T. E. Murphy, "Vector finite difference modesolver for anisotropic dielectric waveguides," *J. Lightw. Technol.*, vol. 26, no. 11, pp. 1423–1431, Jun. 2008.
[55] K. Petermann, "Simple relationship between differential mode delay in optical fibres and the deviation from optimum profile," *Elecron. Lett.*, vol. 14, no. 24, pp. 793–794, Jan. 1978.
[56] G. P. Agrawal, *Fiber-Optic Communication Systems*, (Wiley Series in Microwave and Optical Engineering Series). Hoboken, NJ, USA: Wiley, 2012.

Karthik Choutagunta (Student Member, IEEE) received the B.S. degree in electrical engineering from The University of Texas at Austin, Austin, TX, USA, in 2014, and the M.S. and Ph.D. degrees in electrical engineering from Stanford University, Stanford, CA, USA, in 2016 and 2019, respectively. He has been with Intel Corp., Apple Inc., Facebook Inc., Nokia Bell Laboratories, and a few startup companies. His research interests include various topics in signal processing and machine learning.

Joseph M. Kahn (Fellow, IEEE) received the A.B., M.A., and Ph.D. degrees in physics from the University of California, Berkeley, Berkeley, CA, USA, in 1981, 1983, and 1986, respectively. In 1987–1990, he was with AT&T Bell Laboratories. In 1989, he demonstrated the first successful synchronous (i.e., coherent) detection using semiconductor lasers achieving record receiver sensitivity. Between 1990–2003, he was on the Electrical Engineering and Computer Sciences faculty, Berkeley. He demonstrated coherent detection of QPSK in 1992. In 1999, along with D.-S. Shiu, authored and coauthored the first work on probabilistic shaping for optical communications. In the 1990s and early 2000s, he and collaborators performed seminal work on indoor and outdoor free-space optical communications and multi-input multi-output wireless communications. In 2000, he and K.-P. Ho founded StrataLight Communications, whose 40 Gb/s-per-wavelength long-haul fiber transmission systems were deployed widely by AT&T, Deutsche Telekom, and other carriers. In 2002, Ho and he applied to patent the first electronic compensation of fiber Kerr nonlinearity. StrataLight was acquired by Opnext in 2009. In 2003, he became a Professor of electrical engineering at the E. L. Ginzton Laboratory, Stanford University. He and his collaborators have extensively studied rate-adaptive coding and modulation, as well as digital signal processing for mitigating linear and nonlinear impairments in coherent systems. In 2008, E. Ip and he (and G. Li independently) invented simplified digital backpropagation for compensating fiber Kerr nonlinearity and dispersion. Since 2004, he and his collaborators have studied propagation, modal statistics, spatial multiplexing, and imaging in multimode fibers, elucidating principal modes, and demonstrating transmission beyond the traditional bandwidth-distance limit in 2005, deriving the statistics of coupled modal group delays and gains in 2011, and deriving resolution limits for imaging in 2013. His current research addresses optical frequency comb generators, coherent data center links, rate-adaptive access networks, fiber Kerr nonlinearity mitigation, ultralong-haul submarine links, and optimal free-space transmission through atmospheric turbulence. He was the recipient of the National Science Foundation Presidential Young Investigator Award in 1991.